Journal of Beijing Institute of Technology, 2026, Vol. 35, No. 2

Bearing Fault Diagnosis Based on Gramian Angular Field and Self-Feedback Spiking Neural Networks

Yongping Dan[1]✉, Zhanyang Zhang[1], Zhipeng Liu[1], Xuelong Zhu[2]
(1. School of Integrated Circuits, Zhongyuan University of Technology, Zhengzhou 451191, China;
2. Modern Education Centre, Zhongyuan University of Technology, Zhengzhou 451191, China)

Abstract: In fault diagnosis, feature extraction from vibration signals is widely recognized as the most critical step, as it directly influences the accuracy and reliability of the diagnostic outcomes. To address the limited capability of single-view feature extraction in complex vibration signals and the high economic cost associated with multi-source information fusion, this paper proposes a novel fault diagnosis method based on the Gramian angular field (GAF) and a self-feedback spiking neural network (SF-SNN). The method not only streamlines the network architecture but also enhances the biological plausibility of the SNN model. Initially, GAF is employed to transform the one-dimensional vibration signals collected by sensors into two-dimensional images, effectively preserving the temporal dependencies inherent in the signals. Subsequently, conventional spiking neurons are replaced with self-feedback neurons to enable faster and more precise feature recognition, thereby improving diagnostic performance and classification accuracy. This method inherits the low power consumption and high bionic properties of SNNs while enhancing the efficiency, performance, and robustness of SNN models. It achieved high accuracies of 99.92% and 99.77% on the Case Western Reserve University bearing dataset and the Jiangnan University bearing dataset, respectively. Simultaneously, under noisy conditions (signal-to-noise ratio of –4 dB), it attained accuracies of 80.35% and 80.12%, significantly outperforming other methods. These results fully demonstrate the high accuracy and robust performance of the proposed method on bearing fault diagnosis.

Keywords: Gramian angular field (GAF); spiking neural network; signal processing; spiking self-feedback neuron

1 Introduction

As a cornerstone of industrial production, machinery is deployed across critical sectors including power generation, petrochemicals, and metallurgy. Among numerous components, bearings are particularly critical; their condition — including cracks or faults in different parts — directly impacts equipment performance, efficiency, stability, and service life [1]. Nevertheless, bearings typically operate under complex and harsh conditions, rendering them highly susceptible to damage and degradation. Relevant statistics indicate that over 50% of mechanical failures are attributable to bearing faults [2]. Consequently, achieving high-precision, real-time bearing fault diagnosis is essential for ensuring industrial safety and production continuity. Traditionally, fault identification relied heavily on experienced engineers who analyzed abnormal vibration, acoustic, and temperature signals from engines, gearboxes, and bearings [3,4]. In modern

Manuscript received Oct. 15, 2025; revised Dec. 3, 2025; accepted Dec. 30, 2025. The associate editor coordinating the review of this manuscript was Dr. Lijuan Jia. This research is supported by the Henan Provincial Science and Technology Research Project (No. 242102210006).
✉ Corresponding author. Email: 6100@zut.edu.cn
DOI: 10.15918/j.jbit1004-0579.2025.070

industrial systems, however, there is an increasing demand for intelligent and automated fault diagnosis methods. Such systems not only reduce maintenance costs but also improve detection efficiency, accuracy, and overall operational reliability [5,6].

With the rapid advancement of artificial intelligence (AI), various industries are striving to integrate AI into fault diagnosis methodologies. Unlike conventional fault diagnosis approaches that rely on manual signal analysis, intelligent diagnostic algorithms directly extract meaningful features from large-scale signals [7–10]. A typical intelligent diagnosis process comprises four essential steps: data collection, feature extraction, feature selection, and fault identification [11,12]. Among these, feature extraction involves processing raw sensor data to derive informative features for fault classification. Currently, widely adopted feature extraction techniques include e Gramian angular field (GAF) [13], Markov transition field (MTF) [14], continuous wavelet transform (CWT) [15], and recurrence plot (RP) [16]. These image-coding techniques enhance the representation of signal features, thereby improving fault diagnosis accuracy and efficiency. Different coding methods transform signals from distinct perspectives and dimensions, capturing diverse feature information. Notably, GAF generates information-rich images by converting each pair of data points in a time series into angular values and computing the sums and differences of their sines and cosines, while preserving both the amplitude information of the original signal and its temporal dependencies. This transformation enables network models to comprehensively capture complex fault characteristics while effectively bridging computer vision techniques with fault diagnosis applications.

Spiking neural networks (SNN), recognized as the third generation of neural networks [17], exhibit considerable potential for addressing bearing fault diagnosis. SNN use spike signals as information carriers, effectively simulating the transmission and dynamic behaviors of biological neurons, and integrating information via dynamic synaptic mechanisms to generate rich feature representations [18,19]. Compared with artificial neural networks (ANN), SNN possess an information transmission mechanism analogous to that of the mammalian nervous system, demonstrating superior capabilities in signal processing and biological interpretability [20]. In SNN, information is represented by sparse, discrete spike events, and this sparsity enhances energy efficiency through event-driven computation. In more biologically realistic neuron and synapse models, each neuron operates as a dynamic system capable of spatiotemporal information processing. Additionally, SNN offer benefits such as low energy consumption [21,22]. The event-driven computing paradigm ensures that neurons transmit information only when their membrane potential exceeds a threshold to generate a spike, remaining quiescent otherwise, which significantly reduces unnecessary computations. Leveraging these bionic features and energy efficiency, SNN have been successfully applied in time-series data analysis, object detection, computer vision, and fault classification tasks [23,24]. Nonetheless, SNN development remains at an early stage. Training deep SNN remains a challenge: due to the discontinuity and non-differentiability of spikes, SNN are not suitable for standard backpropagation methods [25], resulting in relatively complex and immature SNN training algorithms. Recently, advances in deep learning have partially addressed this limitation through surrogate gradients, which introduce differentiable approximations during backpropagation to replace non-differentiable spike generation gradients, enabling end-to-end training analogous to ANN. In this study, we introduce spiking self-feedback neurons: by incorporating a feedback loop, The output of the neuron at time step $t-1$ (denoted as $y[t-1]$) is added to the exter-

nal input at the current time step $x[t]$, and their sum serves as the input to the neuron. This design effectively mitigates gradient attenuation during temporal propagation, thereby further optimizing the performance of SNN.

The proposed fault diagnosis method first converts vibration signals into images via the GAF transformation. These images are then encoded into spike signals and processed through the self-feedback spiking neural network (SF-SNN). To further enhance neuronal performance, spiking self-feedback neurons are employed, increasing the sensitivity of the membrane potential to prior inputs and improving the memory capacity of the neurons. Finally, a spike-based classifier is applied to categorize the extracted signal features. The overall framework of the proposed approach is illustrated in Fig. 1. The main contributions of this study are summarized as follows.

1) Design of Gramian angular field transformation: By applying the GAF transformation, vibration signals are converted into images, effectively preserving the temporal correlations of the original signals and retaining rich fault-relevant features. This approach overcomes the limitations of representing complex signal characteristics.

2) Design of spiking self-feedback neurons: By incorporating the influence of the previous-second output of the neuron on its current input, the conventional SNN architecture is optimized, allowing for more efficient extraction of critical information.

3) Proposed SF-SNN model: We design an efficient spiking neural network incorporating spiking self-feedback neurons, which significantly enhances its classification performance while maintaining high computational efficiency.

The remainder of this paper is structured as follows. Section 2 introduces the fundamental principles of SNN-based bearing fault diagnosis, the GAF transformation, and spiking self-feedback neurons. Section 3 presents a detailed description of the proposed methodology. Section 4 evaluates the performance of the proposed approach through extensive experiments conducted on the Jiangnan University (JNU) and Case Western Reserve University (CWRU) bearing datasets. Finally, Section 5 provides a conclusion on the the paper.

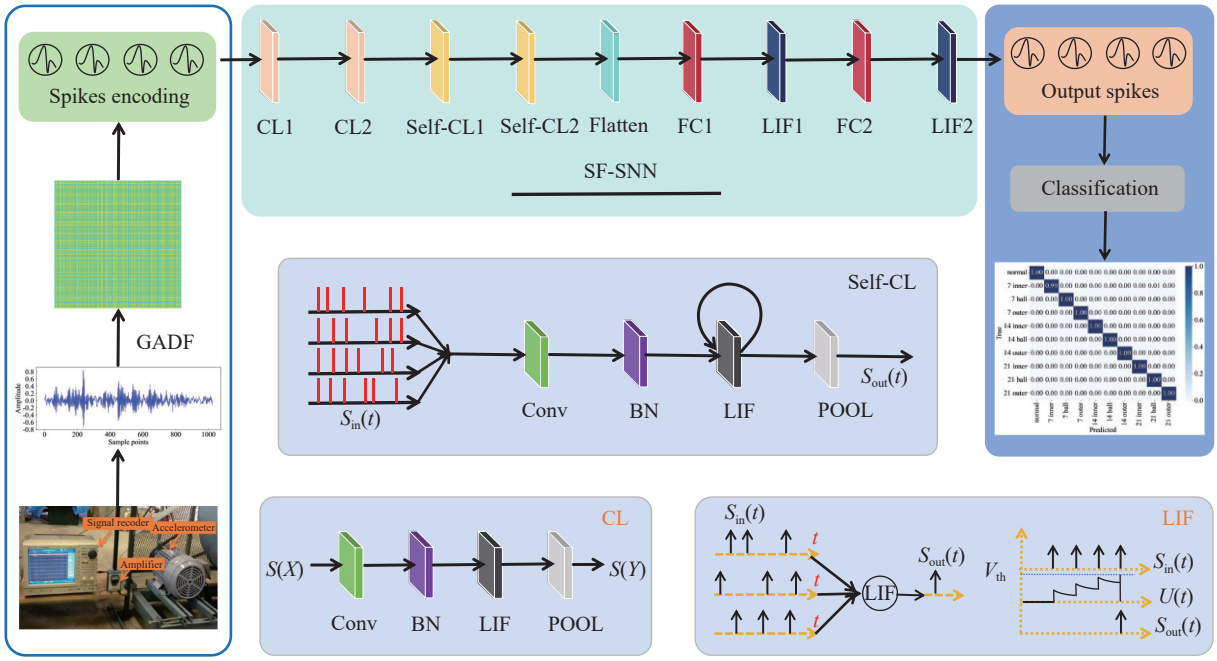

Fig. 1 Overall architecture design

2 Related Work

2.1 Two-Dimensional Feature Image

To overcome the limited feature extraction capabilities of traditional bearing fault diagnosis methods under conditions of scarce samples and strong noise interference, Zhang et al. [26] introduced a convolutional neural network (DFCNN) incorporating two dropout layers and two fully connected layers. The network was trained using two-dimensional (2-D) images generated from one-dimensional (1-D) vibration signals, effectively demonstrating the advantages of 2-D feature representations. Han et al. [27] developed a fault diagnosis approach combining GAF, MTF, and capsule networks, achieving high performance on bearing fault datasets. Gong et al. [28] proposed a lightweight bearing fault detection method based on an enhanced residual network, wherein raw data were converted into time-frequency maps and a crisscross attention mechanism with depthwise separable convolution was integrated into the residual network structure. Shen et al. [29] presented a rolling bearing fault diagnosis approach using GAF and an improved lightweight residual network, embedding a lightweight efficient channel attention (ECA) module after each residual block. Dhungana et al. [30] transformed raw vibration signals into 2-D images using multiple encoding techniques and employed CNNs to classify various types and sizes of bearing faults. Chung et al. [31] converted 1-D signals into recurrence plot (RP) images and applied two deep learning models, achieving excellent results. Zhou et al. [32] proposed a novel rolling bearing fault diagnosis framework combining GAF, convolutional neural networks (CNN), and vision transformer (ViT), achieving average accuracies of 99.79% and 99.63% on two widely used bearing fault datasets. Liu et al. [33] proposed a method integrating Gramian angular difference field (GADF) with dynamic self-calibrated convolution (DSC) for rolling bearing fault diagnosis. Zhang et al. [34] introduced a fault diagnosis approach combining GAF image coding, extreme learning machine (ELM), and CNN, demonstrating fast diagnosis, high accuracy, and strong generalization capabilities. Nevertheless, high-performance ANN require substantial energy consumption [35], limiting their practical applicability on edge devices. To mitigate this issue, bearing fault diagnosis methods based on spiking neural networks have been proposed, offering reduced power consumption.

2.2 SNN in Fault Diagnosis

Chen et al. [36] proposed an innovative framework for bearing fault diagnosis, in which a neural network model incorporating a multi-scale convolutional attention mechanism (MCNN-AM) was trained using a quantized clipping floor shift (QCFS) activation function and subsequently converted into a SNN to achieve low latency and energy-efficient operation. Wu et al. [37] developed a motor fault diagnosis method based on a spiking convolutional neural network with multi-scale decomposed local features; this approach employs discrete wavelet transform (DWT) to extract local features from raw motor fault signals across different temporal and frequency scales. Zhang et al. [38] proposed a convolutional spiking neural network-based method that fully captures the spatiotemporal characteristics of bearing vibration signals. Zuo et al. [39] introduced a multi-scale residual attention SNN (MRA-SNN) with a multi-scale attention encoding module to extract fault features at multiple scales from vibration signals and encode them into spatiotemporal spike sequences without requiring complex preprocessing. Xu et al. [40] developed a deep spiking residual shrinkage network (DSRSN) leveraging attention mechanisms and soft thresholding to achieve high-precision and rapid fault diagnosis under noisy conditions. Additionally, Zuo et al. [41] proposed an SNN-based bearing fault diagnosis method incorporating local mean decomposition (LMD) for feature

extraction. Wang et al. [42] presented an improved spiking neural network (ISNN) for intershaft bearing fault diagnosis, in which raw data were encoded into spike sequences via short-time Fourier transform (STFT)-norm-LIF coding, and spiking neurons were specifically constructed to mitigate information loss during forward propagation. Despite these advances, the absence of a comprehensive theoretical framework and mature training strategies limits the widespread application of SNN in bearing fault diagnosis. Moreover, as bearing vibration signals contain abundant local fault features, existing SNN-based approaches often struggle to capture these details fully. Therefore, exploring emerging computing paradigms is necessary to overcome these limitations.

To overcome the limitations of the aforementioned approaches, the method proposed in this study is designed to efficiently extract local signal features. This approach mitigates noise interference, enhances the memory capacity of the network, and captures fine-grained characteristics of various fault conditions, thereby ensuring high fault diagnosis accuracy while maintaining low energy consumption.

3 Methodology

3.1 GAF Transformation

GAF is a technique for transforming 1-D time-series signals into 2-D images, widely applied for visualization and classification of time-series data. Depending on the trigonometric functions used for encoding, GAF yields two types of feature representations, as shown in Fig. 2: Gramian angular sum field (GASF) images, constructed using cosine function, and Gramian angular difference field (GADF) images, constructed using sine function. In this study, the GADF-based signal processing approach is adopted due to its superior performance, as confirmed by experimental results.

The encoding process is carried out as follows. First, the time series $X = \{x_1, x_2, \cdots, x_n\}$ in the Cartesian coordinate system is normalized to the range $[-1, 1]$ according to Eq. (1), where x_i denotes the i-th sample of the original time series, and $\tilde{x}_i$ represents its normalized value. Subsequently, the normalized values are mapped to angular coordinates ϕ, while the time indices are mapped to radial coordinates r. As a result, the time-domain signal X is transformed into a time series represented in polar coordinates, as expressed in Eq. (2).Where $\tilde{t}_i$ denotes the time stamp, $\tilde{X}$ is the normalized time series, and N serves as a normalization factor for constructing the polar coordinate space.

$$\tilde{x}_i = \frac{x_i - \max X + x_i - \min X}{\max X - \min X} \tag{1}$$

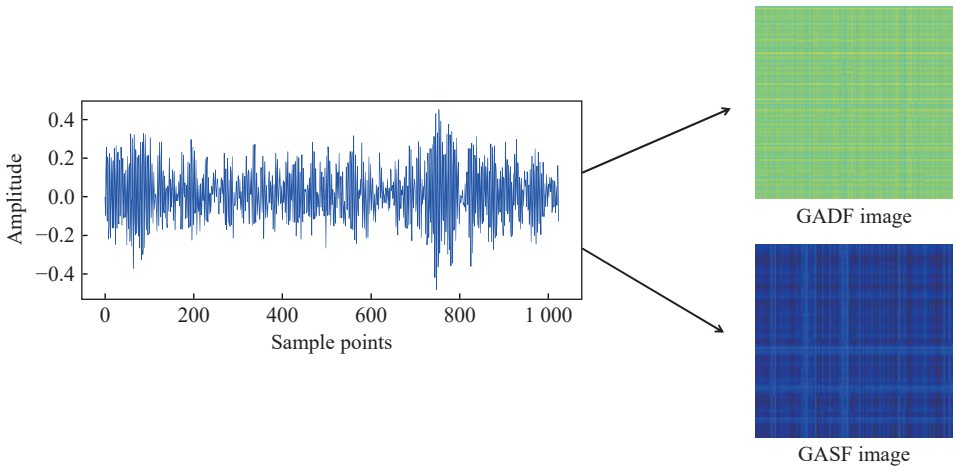

Fig. 2 Diagram of gramian angular field transformation

$$\begin{cases} \phi = \arccos \tilde{x}_i, & -1 \leqslant \tilde{x}_i \leqslant 1, \tilde{x}_i \in \tilde{X} \\ r = \dfrac{t_i}{N}, & t_i \in N \end{cases} \tag{2}$$

After mapping the one-dimensional signal to the polar coordinate system, consider the cosine values of the polar angles sum or polar angle differences between each time series point to identify temporal correlations across different time intervals [43]. Accordingly, as defined in Eq. (1) and Eq. (2), the encoding schemes fall into two categories: GASF and GADF, defined as follows

$$\text{GADF} = \begin{bmatrix} \cos(\phi_1 - \phi_1) & \cdots & \cos(\phi_1 - \phi_n) \\ \cos(\phi_2 - \phi_1) & \cdots & \cos(\phi_2 - \phi_n) \\ \vdots & \vdots & \vdots \\ \cos(\phi_n - \phi_1) & \cdots & \cos(\phi_n - \phi_n) \end{bmatrix} \tag{3}$$

By following the above procedure, the GAF encoding achieves a comprehensive mapping of the original signal while effectively preserving the temporal dependencies among data points, thus minimizing information loss. In summary, this representation provides network models with multi-scale information granularity, thereby improving the overall accuracy of classification tasks.

$$\text{GASF} = \begin{bmatrix} \cos(\phi_1 + \phi_1) & \cdots & \cos(\phi_1 + \phi_n) \\ \cos(\phi_2 + \phi_1) & \cdots & \cos(\phi_2 + \phi_n) \\ \vdots & \vdots & \vdots \\ \cos(\phi_n + \phi_1) & \cdots & \cos(\phi_n + \phi_n) \end{bmatrix} \tag{4}$$

3.2 Spiking Neuron Model

As a fundamental component of the nervous system, biological neurons primarily function to transform a series of synaptic inputs into meaningful streams of action potentials. The typical structure of a neuron consists of four main parts: dendrites, synapses, soma, and axon, as illustrated in Fig. 3(a). Dendrites receive synaptic input signals from other neurons and transmit them to the soma. When these incoming signals alter the membrane potential of the neuron and cause it to exceed a certain threshold, the soma generates a spike, also known as an action potential. This spike then propagates along the axon without attenuation and transmits the signal to downstream neurons via synapses located at the axon terminals.

Spiking neuron models are computational models inspired by biological neurons, and their operational process mimics the information transmission of biological neurons. Each spiking neuron has an internal state variable known as the membrane potential, representing the accumulated charge within the neuron. When the membrane potential reaches a specific threshold, the neuron is activated and emits a spike. The spike is transmitted along the axon to downstream neurons. After reaching the threshold and firing a spike, the membrane potential of the neuron instantaneously resets to a lower level and enters a brief refractory period, during which it is unable to fire again, as illustrated in Fig. 3.

The two most widely adopted mathematical models for spiking neuron membrane potential dynamics are the integrate-and-fire (IF) model and the leaky integrate-and-fire (LIF) model. Both models are described by the following discrete-time equations:

$$H[t] = f(V[t-1], X[t]) \tag{5}$$

$$S[t] = \Theta\left(H[t] - V_{\text{th}}\right) \tag{6}$$

$$V[t] = H[t]\left(1 - S[t]\right) + V_{\text{reset}} S[t] \tag{7}$$

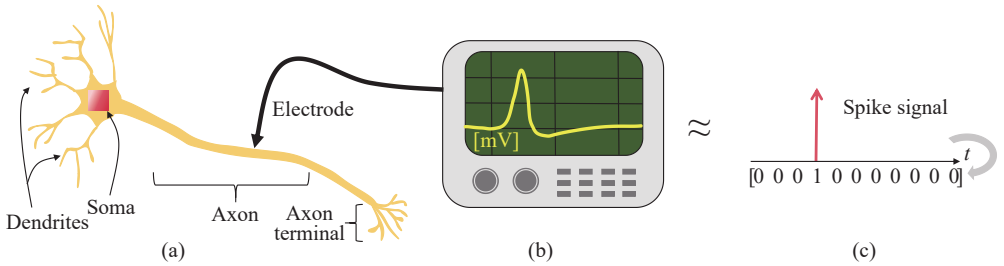

Fig. 3 Mechanism of spike firing: (a) biological neuron; (b) changes in neuron membrane potential; (c) discrete spike event

Here, $X[t]$ denotes the input current at time step t. $H[t]$ and $V[t]$ denote the membrane potential after neuron dynamics and the membrane potential after spike generation at time step t, respectively. $\Theta(x)$ denotes the Heaviside step function, defined by $\Theta(x)=1$ for $x \geqslant 0$ and $\Theta(x)=0$ for $x<0$. $S[t]$ represents the spike output at time step t, taking a value of 1 if a spike occurs and 0 otherwise. V_{reset} denotes the reset potential, and V_{th} denotes the firing threshold. The function $f(\cdot)$ in Eq. (5) characterizes the neuron dynamics, taking different forms for different spiking neuron models, thereby shaping the response of the neuron to input stimuli and determining its spiking behavior [44]. For the IF model, the function f is mathematically expressed as Eq. (8), while for the LIF model, it is expressed by Eq. (9). Eq. (6) and Eq. (7) describe the spike generation and reset processes, which are the same for various spiking neuron models.

$$H[t]=V[t-1]+X[t] \tag{8}$$

$$H[t]=V[t-1]+\frac{1}{\tau}\Big(X[t]-\big(V[t-1]-V_{\text{reset}}\big)\Big) \tag{9}$$

where τ denotes the membrane time constant.

3.3 Spiking Self-Feedback Neurons and Their Neural Networks

The principal structure of the spiking self-feedback neuron is illustrated in Fig. 4. The figure depicts not only the forward connection from the input layer to the output layer in the neuron model but also clearly demonstrates that the output of the neuron influence its own input via a feedback pathway [45]. The underlying principle is as follows. In a spiking self-feedback neuron, let $x[t]$ denote the external input at time t, and $i[t]$ and $y[t]$ represent the input and output of the neuron at time t. By definition, the relationship between input and output is given by: $i[t]=f(x[t],y[t-1])$. Here, f denotes element-wise addition, and with the initial condition $y[-1]=0$, this simplifies to: $i[t]=x[t]+y[t-1]$. From this expression, it is evident that the neuron exhibits a "self-feedback" architecture; that is, the current input depends not only on the external signal $x[t]$ but also on the feedback from its own output $y[t-1]$ at the previous time step. Consequently, even when $t \geqslant 1$ and no external input is present (i.e., $x[t]=0$), the neuron may continue to generate spike outputs, resulting in a self-activation or sustained firing effect. This behavior is highly consistent with the principle of continuous accumulation and decay of membrane potential in biological neurons: when external stimulation ceases, the membrane potential does not immediately return to zero but decays gradually with a characteristic time constant.

Compared to conventional neural networks, networks incorporating spiking self-feedback neurons exhibit enhanced flexibility in their computational mechanisms. Within this context, X and Y denote the input and output of the network, respectively. The conventional network architec-

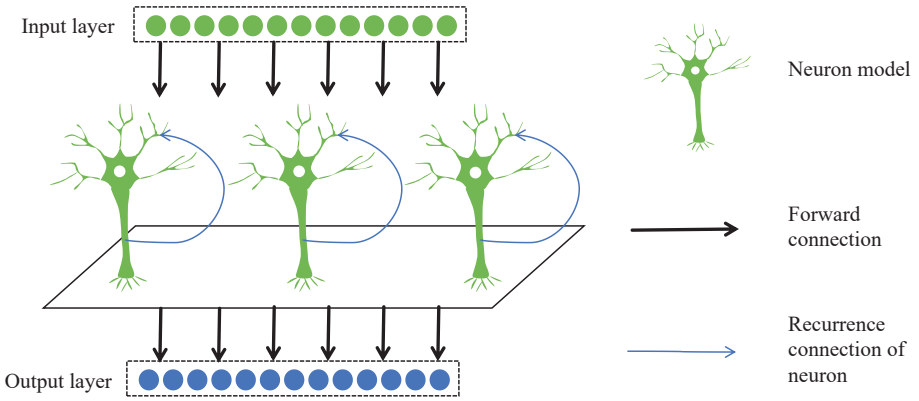

Fig. 4 Schematic diagram of the spiking self-feedback neuron structure

ture illustrated in Fig. 5 (a) relies solely on forward propagation between layers, where the input is sequentially processed through a convolutional layer, a batch normalization layer, a LIF neuron, and a pooling layer. In the self-feedback network architecture depicted in Fig. 5 (b), a recurrent fully connected layer is incorporated between the fully connected layer and the spiking neuron layer, in addition to the conventional feedforward connection. Through the self-feedback operation, historical information and the current input jointly influence the neuron. This self-feedback mechanism confers significant biological plausibility to SNN. It introduces dynamic properties analogous to those observed in the human brain, rendering the behavior of the network comparable to the membrane potential dynamics of real biological neurons. Consequently, SNN gain distinct advantages in simulating cognitive functions of the brain, processing complex signal, and constructing brain-inspired intelligent systems.

Specifically, the primary advantages of incorporating self-feedback neurons into neural networks are as follows:

● Facilitating Memory Function. Because the output of the neuron is fed back to its input, information is preserved across time steps rather than being lost immediately, allowing it to influence subsequent processing. This mechanism thereby endows neurons with short-term memory capabilities, enhancing the network ability to process extract fault-related features.

● Enhancing Model Expressiveness. When processing signals, neurons are able to capture temporal correlations across time steps via self-feedback mechanisms. This enhances the representational power of the network in modeling complex dynamic patterns, rendering it particularly well-suited for tasks, including vibration signal analysis, speech processing, and neuroscientific experimental data interpretation.

● Simulating Self-Regulatory Characteristics of Biological Neurons. In real nervous systems, neurons inherently exhibit self-regulatory mechanisms, including the accumulation and gradual decay of membrane potential as well as the refractory period following spike generation. By incorporating self-feedback connections, SNN are capable of emulating these biological characteristics to a considerable extent, thereby enhancing the consistency of the model with the operational principles of the human brain and improving its interpretability.

● Introducing More Complex Temporal-Dependent Nonlinear Dynamics: Conventional neuron models typically respond to inputs at a single time step or over a restricted temporal window, whereas the incorporation of self-feedback mechanisms endows neurons with increased nonlinearity. This augmented nonlinearity allows an individual neuron to manifest a broader repertoire of dynamic behaviors, such as continuous firing, subthreshold oscillation, and delayed response, greatly enriching the modeling capabilities of the network.

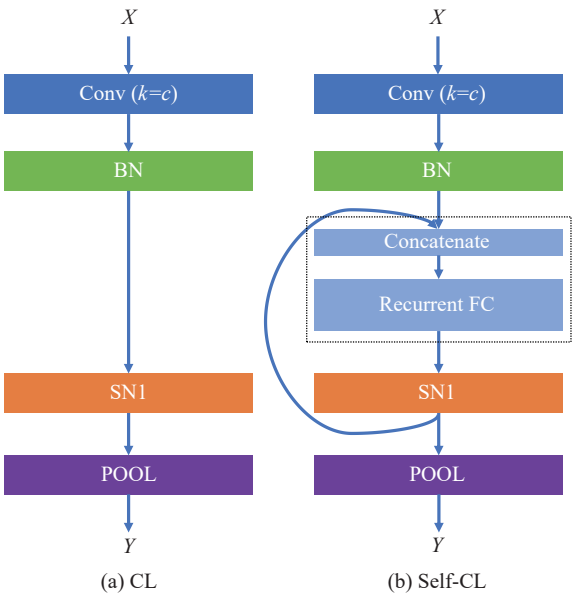

(a) CL (b) Self-CL

Fig. 5 Comparison of two networks: (a) network structure of ordinary spiking neurons; (b) network structure of spiking self-feedback neurons

3.4 Self-Feedback Spiking Neural Network

The basic architecture of the SF-SNN model consists of CL modules, self-CL modules, LIF neurons, and fully connected layers. The network

structures of the CL1 and CL2 modules are shown in Fig. 5 (a), and the network structure of the self-CL module is shown in Fig. 5 (b). We introduce spiking self-feedback neurons into the self-CL module to enhance information transmission and integration. The input to the model is a 2-D image processed by GAF, and the output is the target class. The input layer receives vibration signals transformed by GAF and encodes the images into spike sequences with fixed time steps. The spike sequences propagate forward between network layers. Self-feedback spiking neurons retain and utilize previous information at each time step, enhancing the memory and expression capabilities of input features. The spike output layer accumulates the spikes generated within the time step to realize the final bearing fault category determination. The self-feedback neural network designed in this study is shown in Fig. 6. The final structure of our model consists of two CL modules, two self-CL modules, two layers of LIF neurons, and two fully connected layers. The model structure used is the optimal configuration obtained through experiments.

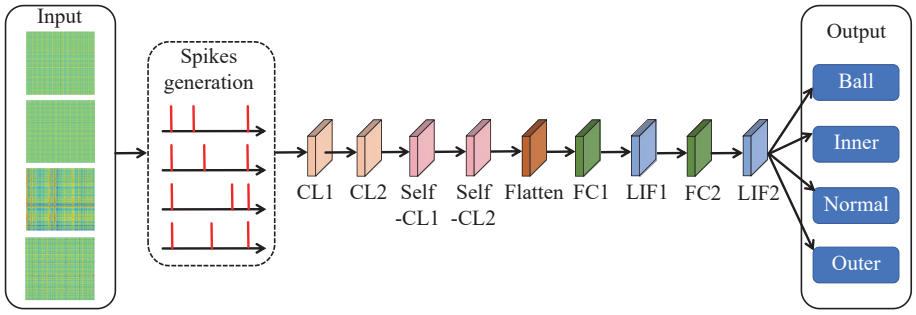

Fig. 6 Network structure of spiking self-feedback neurons

4 Experiments

In this study, the CWRU bearing vibration dataset and the JNU dataset were employed to evaluate the generalization ability and robustness of the proposed model. Considering that rolling bearings in real industrial environments are exposed to varying levels of noise, Gaussian noise was introduced into the datasets to simulate practical operating conditions, thereby evaluating the effectiveness and robustness of the proposed method under noisy environments. So this evaluation will be conducted under five conditions, including no noise and the addition of signal-to-noise ratios (SNR) of –6 dB, –4 dB, –2 dB, and 0 dB, respectively.

All network models in this study were implemented using the PyTorch deep learning framework with Python 3.8. Development was carried out in PyCharm, and experiments were executed on a system equipped with an NVIDIA GeForce RTX 4090 GPU. The hyperparameter settings are summarized in Tab. 1.

Tab. 1 Hyperparameter setup for JNU and CWRU datasets

Hyperparameter	Model
Learning rate	0.001
Optimizer	SGD
Training epochs	200
Time step	4
Batch size	16

4.1 Dataset Description

4.1.1 CWRU Dataset

The test rig used for the CWRU dataset comprises a motor, a torque sensor, a power tester, and a controller, as illustrated in Fig. 7. Accelerometers were mounted on the bearing housings at the motor drive end, fan end, and base to acquire vibration acceleration signals from faulty bearings. Vibration data were acquired at sampling frequencies of 12 kHz and 48 kHz for the drive-end (DE) bearings, while all fan-end (FE) bearing data were sampled at 12 kHz. The dataset includes both normal oper-

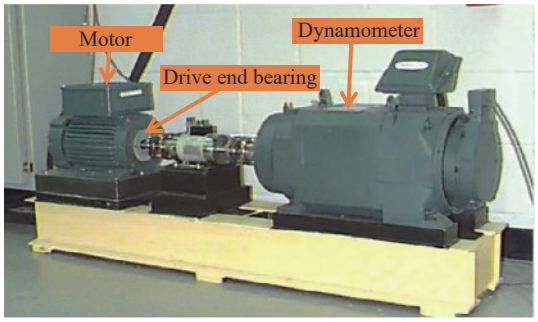

Fig. 7 CWRU rolling bearing experimental platform

ating conditions and various bearing fault conditions, such as defects in the inner ring, outer ring, and rolling elements (balls). Each fault type is represented by three different defect diameters: 0.007 in, 0.014 in, and 0.021 in. Motor loads were set to 0 HP, 1 HP, 2 HP, and 3 HP, corresponding to rotational speeds of 1 797 r/min, 1 772 r/min, 1 750 r/min, and 1 730 r/min, respectively. This dataset offers researchers abundant fault signal data, facilitating the development and validation of various data analysis methods.

Based on industry standard practices, we selected data sampled at 12 kHz from the drive end and categorized them into one healthy state and three fault types: inner ring fault, rolling element fault, and outer ring fault. A total of 10 bearing conditions were tested, comprising one healthy state and nine distinct fault states. Tab. 2 presents the fault classifications of the CWRU dataset along with their corresponding labels. Using the SpikingJelly framework, the acquired data were first transformed into 2-D images via the GADF image coding method. Subsequently, the dataset was trained with a spiking residual neural network employing a sliding window sampling technique, with the window size set to 1 024. The CWRU dataset comprised a total of 10 000 samples, which were partitioned into training, validation, and test sets at an 8:1:1 ratio for model training, validation, and evaluation.

As shown in Fig. 8, for various fault types encoded by GADF images, there are 10 different states (including the normal state), corresponding to each label in Tab. 2.

4.1.2 JNU Dataset

JNU dataset is a publicly available dataset

Tab. 2 Description of CWRU sample categories

Bearing condition	Fault diameter (inch)	Class label
Normal	–	normal
Inner ring	0.007	7inner
Inner ring	0.014	14inner
Inner ring	0.021	21inner
Rolling element	0.007	7ball
Rolling element	0.014	14ball
Rolling element	0.021	21ball
Outer ring	0.007	7outer
Outer ring	0.014	14outer
Outer ring	0.021	21outer

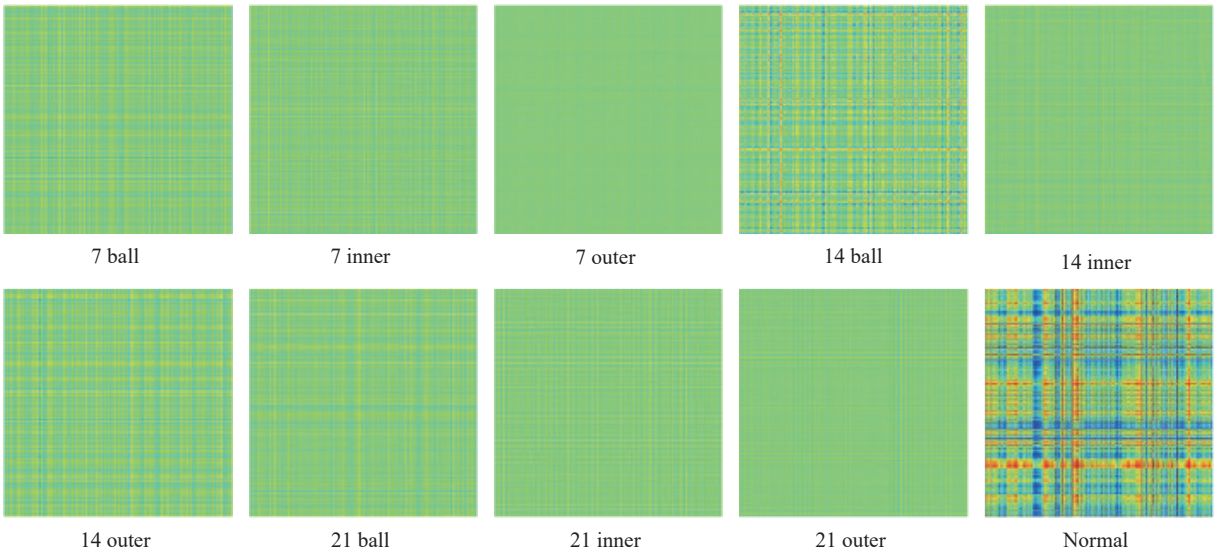

Fig. 8 Fault characteristics of various bearing fault types encoded by GADF on the CWRU dataset

designed for bearing fault diagnosis and predictive maintenance research. It comprises four conditions: inner ring fault (ib), outer ring fault (ob), rolling element fault (tb), and normal state (N). Rotational speeds were set at 600 r/min, 800 r/min, and 1000 r/min. A single accelerometer collected data at a high sampling frequency of 50 kHz, with each sample lasting 20 s. The experimental platform is shown in Fig. 9.

Based on data representativeness, this paper conducts fault diagnosis classification experiments on four types of data from the JNU dataset with a rotational speed of 1000 r/min. Tab. 3 lists the fault settings of the dataset. As with the CWRU dataset, GADF was used to convert the JNU data signals into images. A sliding window method was applied to capture non-overlapping sample sets, each containing 1024 data points. The JNU dataset comprises 4000 samples, divided into 3200 training samples, 400 validation samples and 400 test samples according to an 8:1:1 ratio.

As shown in Fig. 10, corresponding to the various fault types encoded in the GADF images of the JNU bearing dataset, there are four distinct states, each corresponding to a label in Tab. 3.

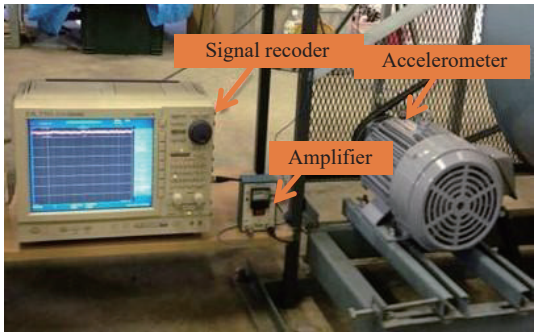

Fig. 9 JNU rolling bearing experimental platform

4.2 Ablation Experiments

Ablation studies were conducted under −4 dB SNR to evaluate the contribution of each component of the proposed method. The experiment is as follows:

w/o SF: Replacing spiking self-feedback neurons with ordinary neurons.

w/o GAF: Removing the GAF signal processing method and using 1-D convolution for feature extraction of 1-D vibration signals.

The ablation results are shown in Tab. 4. using ordinary neurons only achieved an average accuracy of 79.66% on the CWRU dataset and 77.19% on the JNU dataset, demonstrating the contribution of spiking self-feedback neurons to accuracy improvement. Compared with the proposed method, the bearing fault diagnosis method that does not use GAF for 1-D vibration signal processing showed a decrease in recognition accuracy of 2.28% on the CWRU dataset and 2.16% on the JNU dataset. In summary, the bearing fault diagnosis method described in this study is effective.

4.3 Comparative Tests

To demonstrate the superiority of the proposed method, it was compared with published studies on the aforementioned datasets.

4.3.1 Performance with the CWRU Dataset

From the results of the CWRU dataset in Tab. 5, the proposed method exhibits excellent

Tab. 3 Description of JNU sample categories

Fault location	Sample size	Class label
Normal	1000	n
Inner ring	1000	ib
Outer ring	1000	ob
Rolling element	1000	tb

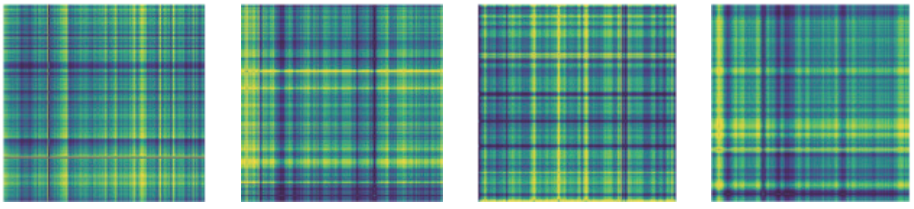

Fig. 10 Fault characteristics of various bearing fault types encoded by GADF on the JNU dataset

Tab. 4 Comparison of ablation experiments (SNR = –4 dB)

Variant	Accuracy (%)	
	CWRU	JNU
w/o SF	79.66	77.19
w/o GAF	81.07	77.96
Our Method	**83.35**	**80.12**

Tab. 5 Comparisons of different methods for the CWRU dataset (no noise)

Network method	Test accuracy (%)
ShuffleNetV2	99.34
MobileNetV2	99.52
VGG16	98.56
ResNet18	99.74
ResNet50	99.85
Swin-T	99.70
ECA_ResNet	99.68
Our Method	**99.92**

classification accuracy, reaching 99.92%. The training and validation accuracy and loss are presented in Fig. 11, and its confusion matrix is shown in Fig. 12. The classification accuracies of the other seven network models were 99.34%, 99.52%, 98.56%, 99.74%, 99.85%, 99.7%, and 96.68% respectively, all of which are lower than our result. As shown in Tab. 6, experiments under noise interference conditions were conducted to obtain the fault diagnostic accuracy of each network model. Under Gaussian white noise levels of –4 dB, –2 dB, 0 dB, 2 dB, and 4 dB, the diagnostic accuracy of the proposed method decreased by 0.31%, 1.02%, 2.34%, 10.32%, and 16.57% respectively, while still exceeding 83%. Particularly under –4 dB noise, the diagnostic accuracy of network models such as ShuffleNetV2 and ResNet50 decreased significantly. In contrast, the decrease in the proposed network was less pronounced. As presented in Fig. 13, demonstrate that the proposed method maintains excellent fault diagnosis performance even under noise interference. This advantage is attributed to the adoption of GADF technology, the unique network structure of SF-SNN, and an efficient feature extraction strategy, which capture key information to achieve more refined and effective feature extraction.

4.3.2 Performance with the JNU Dataset

From the experimental results of the JNU dataset in Tab. 7, our method still dominates in terms of classification accuracy. In the absence of noise, the accuracy reaches 99.77%. Under Gaussian white noise levels of –4 dB, –2 dB, 0 dB, 2 dB, and 4 dB, the classification accuracy of the model was 80.12%, 85.75%, 94.86%, 96.59%, and 97.24%, respectively. Notably, under –2 dB and –4 dB noise, the proposed network outperforms the other seven network models significantly, as shown in Fig. 14. These results confirm the stability and superiority of the proposed method across various datasets, showcasing the substantial effectiveness of combining GAF with spiking self-feedback neurons to enhance neural network performance.

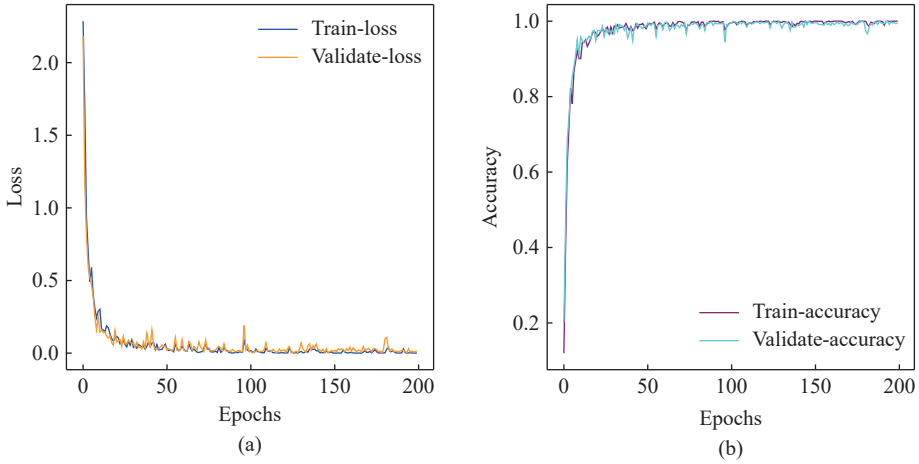

Fig. 11 Training and validation curves of the proposed model without noise: (a) loss curves; (b) accuracy curves

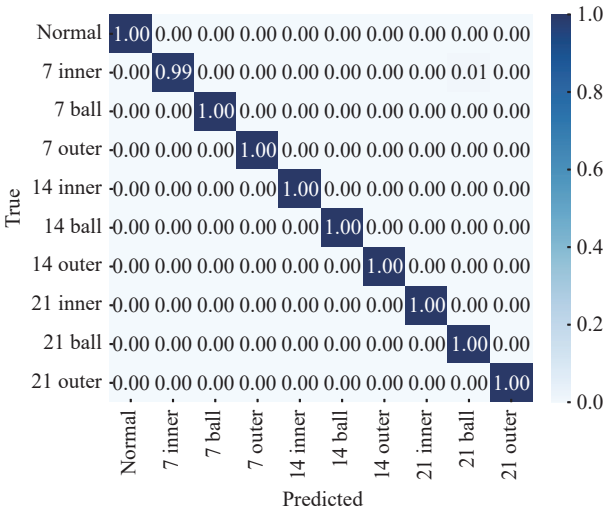

Fig. 12 Confusion matrix of CWRU classification results without noise

Tab. 6 Accuracy of various methods under different noise levels (CWRU)

Network method	SNR (dB)				
	−4	−2	0	2	4
ShuffleNetV2	58.64	81.80	92.35	96.75	97.89
MobileNetV2	67.22	86.52	95.27	98.11	98.35
VGG16	69.98	87.85	95.85	96.30	97.20
ResNet18	67.50	87.60	97.30	98.32	98.97
ResNet50	64.78	86.99	96.80	98.16	99.10
Swin-T	77.36	87.30	97.04	98.20	99.14
ECA_ResNet	68.13	88.24	94.67	97.08	99.08
Our Method	83.35	89.60	97.58	98.90	99.61

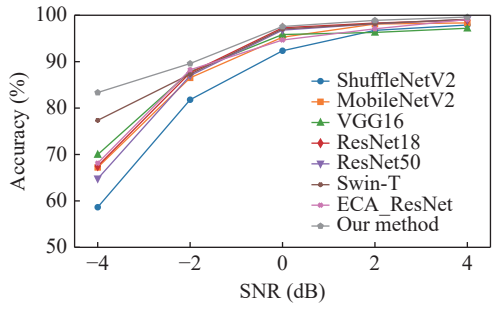

Fig. 13 Accuracy of various methods under different noise levels (CWRU)

5 Conclusion

This study presents a novel bearing fault diagnosis method combining gramian angular field signal processing with SF-SNN. gramian angular field converts time-series data into images while preserving salient feature information, making it

Tab. 7 Accuracy of various methods under different noise levels (JNU)

Network method	SNR (dB)					No noise
	−4	−2	0	2	4	
ShuffleNetV2	53.29	76.99	91.44	94.90	96.80	98.20
MobileNetV2	64.25	82.42	93.39	96.17	96.65	98.41
VGG16	68.80	84.37	93.70	95.20	96.20	97.65
ResNet18	66.97	84.51	94.46	96.38	97.06	98.63
ResNet50	61.54	82.03	94.10	96.30	97.19	98.70
Swin-T	76.69	83.60	94.53	96.44	97.20	98.52
ECA_ResNet	65.10	84.70	92.85	95.29	96.83	98.54
Our Method	80.12	85.75	94.86	96.59	97.24	99.77

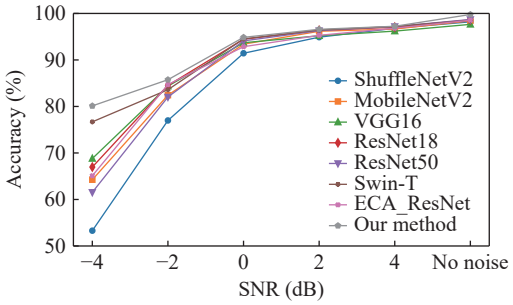

Fig. 14 Accuracy of various methods under different noise levels (JNU)

suitable for processing nonstationary signals such as bearing vibration signals. Furthermore, incorporating spiking self-feedback neurons into SF-SNN enhances both accuracy and robustness. Experiments on the CWRU and JNU bearing datasets show that the proposed method achieves superior fault classification and generalization performance, outperforming other approaches. The results demonstrate the effectiveness of the method in overcoming the challenges posed by scarce or imbalanced data, thereby improving the reliability and practicality of bearing fault diagnosis in industrial applications.

The proposed method achieves high diagnostic accuracy on the CWRU dataset under different noise conditions: 99.92% in noiseless conditions, 89.6% under −2 dB noise, and 83.35% under −4 dB noise. On the JNU dataset, it attains an accuracy range of 80.12% to 99.77% across noiseless conditions and various SNR levels. Compared with traditional machine learning, deep learning, and other graph-based neural net-

work models, the proposed method effectively mitigates the impact of noise, making it more suitable for practical bearing fault diagnosis.

Despite these promising outcomes, the method currently relies on computationally intensive training and has not yet been tested across all types of industrial machinery or extreme operating conditions. Future work will focus on optimizing network efficiency, extending the model to a wider range of signal and information processing domains.

References:

[1] X. Li and W. Zhang,"Deep learningbased partial domain adaptation method on intelligent machinery fault diagnostics," *IEEE Transactions on Industrial Electronics*, vol. 68, no. 5, pp. 4351-4361, 2020.

[2] W. Wang and H. Lee,"An energy kurtosis demodulation technique for signal denoising and bearing fault detection," *Measurement Science and Technology*, vol. 24, no. 2, pp. 025601, 2013.

[3] Z. Li, Y. Yan, X. Wang, Y. Ge, and L. Meng,"A survey of deep learning for industrial visual anomaly detection," *Artificial Intelligence Review*, vol. 58, no. 9, pp. 1-82, 2025.

[4] Z. Li, Y. Ge, and L. Meng,"A multiscale information fusion framework with interaction-aware global attention for industrial vision anomaly detection and localization," *Information Fusion*, vol. 124, pp. 103356, 2025.

[5] Z. Li, Y. Ge, X. Wang, X. Yue, and L. Meng, "Industrial anomaly detection via teacher student network, " in *2023 International Conference on Advanced Mechatronic Systems (ICAMechS)*, pp. 1-5, 2023.

[6] Z. Li, Y. Ge, X. Wang, and L. Meng,"3d industrial anomaly detection via dual reconstruction network," *Applied Intelligence*, vol. 54, no. 20, pp. 9956-9970, 2024.

[7] W. Zhang, C. Li, G. Peng, Y. Chen, and Z. Zhang,"A deep convolutional neural network with new training methods for bearing fault diagnosis under noisy environment and different working load," *Mechanical systems and signal processing*, vol. 100, pp. 439-453, 2018.

[8] Z. Li, Y. Ge, X. Yue, and L. Meng,"Mcad: Multiclassification anomaly detection with relational knowledge distillation," *Neural Computing and Applications*, vol. 36, no. 23, pp. 14, 2024.

[9] Z. Li, H. Li, and L. Meng,"Model compression for deep neural networks: A survey," *Computers*, vol. 12, no. 3, pp. 60, 2023.

[10] X. Yue, H. Li, Y. Fujikawa, and L. Meng, "Dynamic dataset augmentation for deep learning-based oracle bone inscriptions recognition," *ACM Journal on Computing and Cultural Heritage*, vol. 15, no. 4, pp. 1-20, 2022.

[11] D. S. Huang, Systematic theory of neural networks for pattern recognition, *Pub*lishing House of Electronic Industry of China, Beijing, vol. 201, 1996.

[12] H. Li, Z. Wang, X. Yue, W. Wang, H. Tomiyama, and L. Meng,"An architecture-level analysis on deep learning models for low-impact computations," *Artificial Intelligence Review*, vol. 56, no. 3, pp. 1971-2010, 2023.

[13] Z. Zeng, J. Yang, Y. Wei, X. Wang, and P. Wang, "Fault detection of flexible dc distribution network based on gaf and improved deep residual network," *Journal of Electrical Engineering & Technology*, vol. 19, no. 7, pp. 3935-3945, 2024.

[14] M. Wang, W. Wang, X. Zhang, and H. H. C. Iu,"A new fault diagnosis of rolling bearing based on markov transition field and CNN," *Entropy*, vol. 24, no. 6, pp. 751, 2022.

[15] N. Diao, Z. Wang, H. Ma, and W. Yang,"Fault diagnosis of rolling bearing under variable working conditions based on CWT and t-resnet," *Journal of Vibration Engineering & Technologies*, vol. 11, no. 8, pp. 3747-3757, 2023.

[16] X. Liu, L. Xia, J. Shi, L. Zhang, L. Bai, and S. Wang,"A fault diagnosis method of rolling bearing based on improved recurrence plot and convolutional neural network," *IEEE Sensors Journal*, vol. 23, no. 10, pp. 10, 2023.

[17] W. Maass,"Networks of spiking neurons: the third generation of neural network models," *Neural networks*, vol. 10, no. 9, pp. 1659-1671, 1997.

[18] Z. Li and L. Meng,"Deep spiking neural networks for image classification," *International Journal of Human Factors Modelling and Simulation*, vol. 8, no. 1, pp. 21-35, 2023.

[19] Y. Ge, Z. Li, X. Yue, H. Li, and L. Meng,"Dataset purification-driven lightweight deep learning model construction for empty-dish recycling robot," *IEEE Transactions on Emerging Topics in Computational Intelligence*, vol. 9, no. 5, pp. 3325-3340, 2025.

[20] Y. Guo, W. Peng, Y. Chen, L. Zhang, X. Liu, X. Huang, and Z. Ma,"Joint ASNN: Joint training of

artificial and spiking neural networks via self-distillation and weight factorization," *Pattern Recognition*, vol. 142, pp. 109639, 2023.

[21] K. Roy, A. Jaiswal, and P. Panda,"Towards spike-based machine intelligence with neuromorphic computing," *Nature*, vol. 575, no. 7784, pp. 607-617, 2019.

[22] Y. Dan, C. Sun, H. Li, and L. Meng,"Adaptive spiking neuron with population coding for a residual spiking neural network," *Applied Intelligence*, vol. 55, no. 4, pp. 288, 2025.

[23] Y. Ding, L. Zuo, M. Jing, P. He, and Y. Xiao, "Shrinking your timestep: Towards low-latency neuromorphic object recognition with spiking neural networks, " in *Proceedings of the AAAI Conference on Artificial Intelligence*, vol. 38, no. 10, pp. 11811-11819, 2024.

[24] Y. Hu, L. Deng, Y. Wu, M. Yao, and G. Li, "Advancing spiking neural networks toward deep residual learning," *IEEE transactions on neural networks and learning systems*, vol. 36, no. 2, pp. 2353-2367, 2024.

[25] E. O. Neftci, H. Mostafa, and F. Zenke,"Surrogate gradient learning in spiking neural networks: Bringing the power of gradient-based optimization to spiking neural networks," *IEEE Signal Processing Magazine*, vol. 36, no. 6, pp. 51-63, 2019.

[26] J. Zhang, S. Yi, G. Liang, G. Hongli, H. Xin, and S. Hongliang,"A new bearing fault diagnosis method based on modified convolutional neural networks," *Chinese Journal of Aeronautics*, vol. 33, no. 2, pp. 439-447, 2020.

[27] B. Han, H. Zhang, M. Sun, and F. Wu,"A new bearing fault diagnosis method based on capsule network and markov transition field/gramian angular field," *Sensors*, vol. 21, no. 22, pp. 7762, 2021.

[28] L. Gong, C. Pang, G. Wang, and N. Shi, "Lightweight bearing fault diagnosis method based on improved residual network," *Electronics*, vol. 13, no. 18, pp. 3749, 2024.

[29] J. Shen, Z. Wu, Y. Cao, Q. Zhang, and Y. Cui, "Research on fault diagnosis of rolling bearing based on gramian angular field and lightweight model," *Sensors*, vol. 24, no. 18, pp. 5952, 2024.

[30] H. Dhungana, S. K. Mukhiya, P. Dhungana, and B. Karic, "Deep learning-based fault identification in condition monitoring, " in *International Conference on Applications in Electronics Pervading Industry, Environment and Society*, pp. 418-428, 2024.

[31] K. J. Chung and C. W. Lin,"Condition monitoring for fault diagnosis of railway wheels using recurrence plots and convolutional neural networks (RP-CNN) models," *Measurement and Control*, vol. 57, no. 3, pp. 330-338, 2024.

[32] Z. Zhou, Q. Ai, P. Lou, J. Hu, and J. Yan,"A novel method for rolling bearing fault diagnosis based on gramian angular field and CNN-VIT," *Sensors*, vol. 24, no. 12, pp. 3967, 2024.

[33] C. Liu, J. Bai, L. Xue, and Z. Xue,"Rolling bearing fault diagnosis method based on gramian angular difference field and dynamic self-calibrated convolution module," *PloS one*, vol. 19, no. 12, pp. e0314898, 2024.

[34] Y. Zhang, L. Shang, H. Gao, Y. He, X. Xu, and Y. Chen,"A new method for diagnosing motor bearing faults based on gramian angular field image coding and improved CNN-ELM," *IEEE Access*, vol. 11, pp. 11, 2023.

[35] J. Feldmann, N. Youngblood, C. D. Wright, H. Bhaskaran, and W. H. Pernice,"All-optical spiking neurosynaptic networks with self-learning capabilities," *Nature*, vol. 569, no. 7755, pp. 208-214, 2019.

[36] X. Chen, J. Li, A. Yu, B. Cai, Q. Wu, and M. Xia,"Ultra-low latency ANN-SNN conversion for bearing fault diagnosis," *IEEE Transactions on Instrumentation and Measurement*, vol. 74, pp. 3518010, 2025.

[37] G. Wu, Z. Huang, Z. Long, F. Huang, M. H. Wang, and X. Zhang,"Motor fault diagnosis method based on spiking convolutional neural network with multi-scale decomposition local features," *ISA transactions*, vol. 164, pp. 271-283, 2025.

[38] C. Zhang, Z. Xiao, and Z. Sheng,"A bearing fault diagnosis method based on a convolutional spiking neural network with spatial-temporal feature-extraction capability," *Transportation Safety and Environment*, vol. 5, no. 2, pp. tdac050, 2023.

[39] L. Zuo, Y. Ding, M. Jing, K. Yang, B. Chen, and Y. Yu, "Toward end-toend bearing fault diagnosis for industrial scenarios with spiking neural networks, " *arXiv preprint*, arXiv: 2408.11067, 2024.

[40] Z. Xu, Y. Ma, Z. Pan, and X. Zheng,"Deep spiking residual shrinkage network for bearing fault diagnosis," *IEEE Transactions on Cybernetics*, vol. 54, no. 3, pp. 1608-1613, 2022.

[41] L. Zuo, L. Zhang, Z. H. Zhang, X. L. Luo, and Y. Liu,"A spiking neural networkbased approach to bearing fault diagnosis," *Journal of Manufacturing Systems*, vol. 61, pp. 714-724, 2021.

[42] J. Wang, T. Li, C. Sun, R. Yan, and X. Chen,"Improved spiking neural network for inter-

shaft bearing fault diagnosis," *Journal of Manufacturing Systems*, vol. 65, pp. 208-219, 2022.

[43] Z. Wang and T. Oates, "Imaging timeseries to improve classification and imputation, " *arXiv preprint*, arXiv: 1506.00327, 2015.

[44] Y. Dan, Z. Wang, H. Li, and J. Wei,"Sasnn: spiking attention neural network for image classification," *PeerJ Computer Science*, vol. 10, pp. e2549, 2024.

[45] B. Yin, F. Corradi, and S. M. Bohté, "Effective and efficient computation with multiple-timescale spiking recurrent neural networks, " in *International Conference on Neuromorphic Systems 2020*, pp. 1-8, 2020.

Yongping Dan received the Ph.D. degree in Huazhong University of Science and Technology, Wuhan, China, in 2008. Now he is a teacher in Zhongyuan University of Technology. His research interests include deep spiking neural networks and brain-Inspired computing.

Zhanyang Zhang is currently pursuing a master's degree in control engineering at Zhongyuan University of Technology. His research interests are mainly focused on bearing failure diagnosis.

Zhipeng Liu is currently pursuing a master's degree in control engineering at Zhongyuan University of Technology. His research interests are mainly focused on field programmable gate array.

Xuelong Zhu is a teacher in Zhongyuan University of Technology. His research interests include smart clothing and fabric defect detection.